Eur Radiol (2016) 26:2019–2029
DOI 10.1007/s00330-015-4045-0

MAGNETIC RESONANCE

Novel application of chemical shift gradient echo in- and opposed-phase sequences in 3 T MRI for the detection of H-MRS visible lipids and grading of glioma

Norlisah Ramli[1] · Azua Mohd Khairy[2] · Pohchoo Seow[1] · Li Kuo Tan[1] · Jeannie Hsiu Ding Wong[1] · Dharmendra Ganesan[3] · Kartini Rahmat[1]

Received: 3 July 2015 / Revised: 19 August 2015 / Accepted: 23 September 2015 / Published online: 11 November 2015

Abstract

Objectives We evaluated the feasibility of using chemical shift gradient-echo (GE) in- and opposed-phase (IOP) imaging to grade glioma.

Methods A phantom study was performed to investigate the correlation of ^{1}H MRS-visible lipids with the signal loss ratio (SLR) obtained using IOP imaging. A cross-sectional study approved by the institutional review board was carried out in 22 patients with different glioma grades. The patients underwent scanning using IOP imaging and single-voxel spectroscopy (SVS) using 3T MRI. The brain spectra acquisitions from solid and cystic components were obtained and correlated with the SLR for different grades.

Results The phantom study showed a positive linear correlation between lipid quantification at 0.9 parts per million (ppm) and 1.3 ppm with SLR ($r=0.79–0.99$, $p<0.05$). In the clinical study, we found that SLR at the solid portions was the best measure for differentiating glioma grades using optimal cut-points of 0.064 and 0.086 with classification probabilities for grade II ($S_{II}=1$), grade III ($S_{III}=0.50$) and grade IV ($S_{IV}=0.89$).

Conclusions The results underscore the lipid quantification differences in grades of glioma and provide a more comprehensive characterization by using SLR in chemical shift GE IOP imaging. SLR in IOP sequence demonstrates good performance in glioma grading.

Key Points

- *Strong correlation was seen between lipid concentration and SLR obtained using IOP*
- *IOP sequence demonstrates significant differences in signal loss within the glioma grades*
- *SLR at solid tumour portions was the best measure for differentiation*
- *This sequence is applicable in a research capacity for glioma staging armamentarium*

Keywords Lipid phantom · Magnetic resonance spectroscopy · Volume under the receiver operating curve surface · Glioma classification · In- and opposed-phase imaging

✉ Norlisah Ramli
norlisahramli@gmail.com

Azua Mohd Khairy
drazua79@yahoo.com.my

Pohchoo Seow
swpohchoo@gmail.com

Li Kuo Tan
lktan@ummc.edu.my

Jeannie Hsiu Ding Wong
jeannie_wong80@um.edu.my

Dharmendra Ganesan
drdharmen@gmail.com

Kartini Rahmat
katt_xr2000@yahoo.com

[1] Department of Biomedical Imaging, University Malaya Research Imaging Centre, University of Malaya, 59100 Kuala Lumpur, Malaysia

[2] Department of Radiology, Sultan Ismail Hospital, Jalan Persiaran Mutiara Emas Utama, Taman Mount Austin, 81100 Johor Bahru, Malaysia

[3] Division of Neurosurgery, Department of Surgery, University of Malaya, 59100 Kuala Lumpur, Malaysia

Introduction

Glioma describes any tumour arising from the interstitial tissue of the brain [1]. The grading of gliomas is important, as it

directs further management and determines the prognosis of the patient. Brain biopsy for histopathologic grading is currently the gold standard for the grading of gliomas. However, it is an invasive procedure and poses certain risks to patients, such as infection and bleeding, in addition to the inherent possibility of sampling error during biopsy. One of the main concerns with stereotactic biopsy, particularly with regard to gliomas, is the accuracy of the histological results, considering the occurrence of heterogeneity within the tumour itself. Magnetic resonance imaging (MRI) is an established technique for biopsy planning and characterization of gliomas [2]. MRI has the ability to image the entire lesion and the adjacent brain tissue for glioma evaluation, and provides valuable information, including contrast enhancement, oedema, haemorrhage, necrosis, and mass effect, for characterization of tumour aggressiveness. Uptake of contrast in the tumour indicates blood–barrier breakdown or neovascularity, which is a feature of high-grade glioma. Grading of gliomas using conventional MRI images is often carried out as part of the preoperative assessment in cases of glioma, which may or may not be done in conjunction with magnetic resonance spectroscopy (MRS). However, glioma grading using conventional MRI is sometimes unreliable due to the high false-positive rates arising from the variability in tumour features [2, 3].

Over the last two decades, MRS has been increasingly used for the grading of gliomas. Multiple previous studies have corroborated and validated the relationship between the metabolites detected by MRS and glioma grading [3–6]. Lipids are one of the recognized metabolites consistently associated with gliomas; previous studies [3–6] have utilized the mobile lipid signals at 1.3 and 0.9 ppm as reference points. Although MRS is considered a robust method for glioma grading [6], it has several drawbacks. Multi-voxel MRS requires a long acquisition time (6–10 minutes), which may give rise to motion artefacts and patient discomfort. Image acquisition and spectral differentiation may suffer from magnetic susceptibility artefacts formed by the adjacent bones and haemorrhage, motion artefacts and poor shimming [3]. Single-voxel spectroscopy (SVS), in particular, not only requires expensive software, but is time-consuming for post-processing and result interpretation [7].

The chemical shift in- and opposed-phase (IOP) sequence is one of the gradient-echo (GE) MRI sequences, and it has been clinically utilized for the detection of lipids in various conditions, including adrenal adenoma, renal angiomyolipoma, bone marrow pathology and whole-body fat quantification [8–12]. A recent study has also shown its usefulness in the detection of mobile lipids in intracranial lesions, including gliomas [13]. Elevated lipid levels in gliomas have been reported in various studies [14]. In high-grade gliomas, elevated lipid levels appear as a higher signal loss in the opposed-phase images. In this work, we attempt to take advantage of this physical phenomenon for grading of gliomas based on lipid levels. Other advantages of this imaging sequence include shorter acquisition time (approximately 1 min), which is an advantage over MRS acquisition. This sequence is also not susceptible to artefacts formed by adjacent bones and does not require expensive software applications [7, 15, 16].

In this study, we investigated the feasibility of using the IOP imaging sequence to grade glioma. This work is divided into two parts. The first involves a phantom study in which parameters obtained using the IOP sequence are correlated to lipid quantification using MRS. In the second section, the feasibility of this method for glioma grading is investigated in a cohort of 22 patients diagnosed with various stages of glioma.

Materials and methods

Phantom study

Few lipid phantom studies have been carried out in which the IOP sequence has been used for characterization [8, 13, 17]. To the best of the authors' knowledge, no studies conducted to date have used this sequence to investigate the correlation of lipid components (ppm) obtained from SVS with lipid concentration (%). In the current work, a lipid phantom was constructed using SMOFlipid® 20 % (Fresenius Kabi, Richmond Hill, Ontario, Canada), an emulsion used for infusion containing soya oil, medium-chain triglycerides, olive oil and fish oil. The lipid phantom attempts to model the effects of low-lipid-fraction tumours, such as gliomas, in an IOP sequence in contrast to high-lipid-fraction tumours such as lipomas.

The lipid phantom was constructed using ten 50-ml (6.7-cm height and 4.2-cm inner diameter) cylindrical bottles placed within a larger rectangular ($25.2\times9.0\times7.5$ cm^3) container (Fig. 1). To prepare the solution for injection, the lipid in SMOFlipid® 20 % was further diluted with water to obtain nine 40-ml lipid phantom dilutions ranging from 20 to 1 %. A tenth bottle was filled with pure water to act as a control. The ten bottles were then submerged in a gelatin bath contained in the rectangular container in order to augment magnetic field homogeneity.

Coronal images of these phantoms were acquired with a standard GE IOP sequence on a 3T MRI unit (Signa HDx; GE Healthcare, Milwaukee, WI) using a dedicated head coil. Imaging parameters were as follows: 150 ms repetition time; 2.4 ms echo time for the in-phase, 5.8 ms echo time for the opposed-phase; flip angle of 80°; number of averages=1; 250×250 mm^2 field of view; matrix size of 256×256; and 5-mm slice thickness. Total scan time was 1 min 20 s.

Single-voxel spectroscopy (SVS) was then performed using a point-resolved single-voxel spectroscopy (PRESS) probe-p sequence with a short echo time of 35 ms and

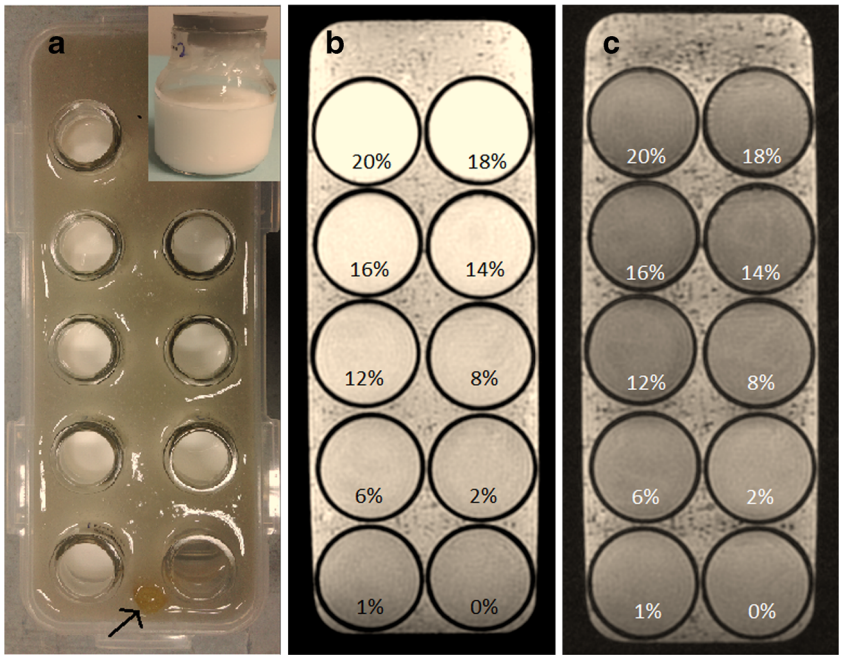

Fig. 1 (a) Experimental setup for cylindrical bottles containing nine lipid dilutions and one control phantom submerged in a gelatin bath, with *inset photo* showing the actual cylindrical bottle used to contain the lipids. Fish oil *(arrow)* was used as a marker to distinguish the arrangement of the phantom in the MRI image. (b) In-phase and (c) opposed-phase images of the lipid phantom. Lipids at 0 % indicates pure water, which acts as a control

repetition time of 2000 ms. The axial, coronal and sagittal multiplanar reconstructions of 3D T1 post-gadolinium fluid attenuation inversion recovery (FLAIR) images were used to position a single voxel in the centre of the phantom, well away from the side walls, with a volume of interest (VOI) of $1\times1\times1$ cm^3.

For analysis, the signal intensity (SI) of the IOP images was measured using the OsiriX DICOM (v5, Pixmeo Sarl, Switzerland). Three 3.0-mm^3 round regions of interest (ROIs) were placed in the centre of the phantom in the in-phase and opposed-phase images, and the mean SI values were obtained. The signal loss ratios (SLRs) were calculated using the following equation [18]:

$$\text{Signal loss ratio (SLR)} = \frac{\text{Signal}_{\text{in-phase}} - \text{Signal}_{\text{opposed-phase}}}{\text{Signal}_{\text{in-phase}}}$$

The raw data (P-files) obtained from the SVS measurements were post-processed using LCModel (v6.2, LCMODEL Inc., Ontario, Canada) [19] to acquire the lipid spectra of each dilution, where peaks of lipid components were depicted at 0.9, 1.3, 1.6, 2.1, 2.3 and 2.8 ppm. The LCModel settings of SPTYPE='lipid-8' was chosen as the basis set to adjust for spectra with lipid and water signals only. The Cramér Rao lower bound (CRLB) [20] was used to quantify the accuracy of the metabolite identification. Lipid concentrations with CRLB >20 % [19] were excluded from analysis. Statistical analysis was carried out using SPSS version 22 statistical software (IBM Corp., Armonk, NY). The Pearson correlation test was used to test the correlation between the SLR and various lipid concentrations, and statistical significance was declared at $p<0.05$.

Clinical study

Full ethical approval was obtained from the local institutional review board committee. All patients provided written informed consent. This was a cross-sectional study of 22 patients with histologically proven gliomas who were initially referred to our centre over a period from April 2011 to April 2015 for an assessment of intracranial space lesions. With the use of a 3T MRI unit equipped with a dedicated head coil, a standard tumour protocol was performed, with an additional chemical shift GE IOP sequence obtained before contrast was administered, followed by an SVS sequence after contrast administration. Similar parameters were adopted for the IOP sequence in the phantom study. None of the recruited glioma patients had received any treatment prior to the study. SVS was performed for the solid and cystic components of the lesion using a 1500-ms repetition time, 35-ms echo time and a VOI of $1\times1\times1$ cm^3. The solid portion was considered as the portion of the tumour exhibiting an isointense signal on T1-weighted (T1W) images and iso- to hyperintense signal on T2-weighted (T2W) images, regardless of the presence or absence of tumour enhancement. The necrotic or cystic portion was considered the portion of the tumour exhibiting a hypointense signal on T1W images and hyperintense signal on T2W images, which is similar to cerebrospinal fluid. Raw data (P-files) obtained from the SVS measurements were post-processed using a method similar to that used in the phantom study.

A single neuroradiologist (KR) with 7 years of post-specialisation experience and one trainee radiologist (AMK) performed measurements of the SI of IOP images using the

OsiriX DICOM. The solid and cystic components were identified, and three ROIs were placed on the solid portion and another three on the cystic portion (if available) in the in-phase images. Placement of three ROIs was made to account for variation in the internal heterogeneity of the intra-axial masses. Opposed-phase images were then obtained with identical placement of the ROIs (Figs. 2 and 3). ROIs were kept to around 3.0 mm^3 in size. The mean SLRs (for solid and cystic portions) were subsequently calculated and recorded.

Statistical analysis

Kruskal–Wallis and Mann–Whitney *U* tests were used to determine significant differences in lipid concentration and SLR among the lesions of various tumour grades and across all tumour grades, respectively. A Pearson correlation test was used to establish the correlation between the SLR and lipid concentrations for the phantom study. Statistical significance was declared at $p<0.05$. A three-group analysis was performed in order to differentiate grades II, III and IV using R software (R Foundation for Statistical Computing, Vienna, Austria) [21]. The summary measures for the three grades were performed based on the volume under the surface (VUS) of the receiver operating characteristics (ROC) curve, in order to evaluate the discriminative ability of the SVS and SLR. VUS analysis was performed on lipid components that demonstrated statistical significance in Kruskal–Wallis tests.

Histological analysis

The biopsy specimens were evaluated using gold-standard histopathological analysis following the World Health Organization (WHO) guidelines [22]. According to guidelines, astrocytic tumour can be categorized as diffuse astrocytoma, anaplastic astrocytoma or malignant glioblastoma (GBM) by grades II, III or IV, respectively. We followed this designation and graded tumours accordingly.

Results

Phantom study

Table 1 depicts the lipids detected in the phantom by LCModel at selected lipid concentrations. Distinct lipid signals were measurable at around 0.9 ppm (Lip0.9 ppm) and

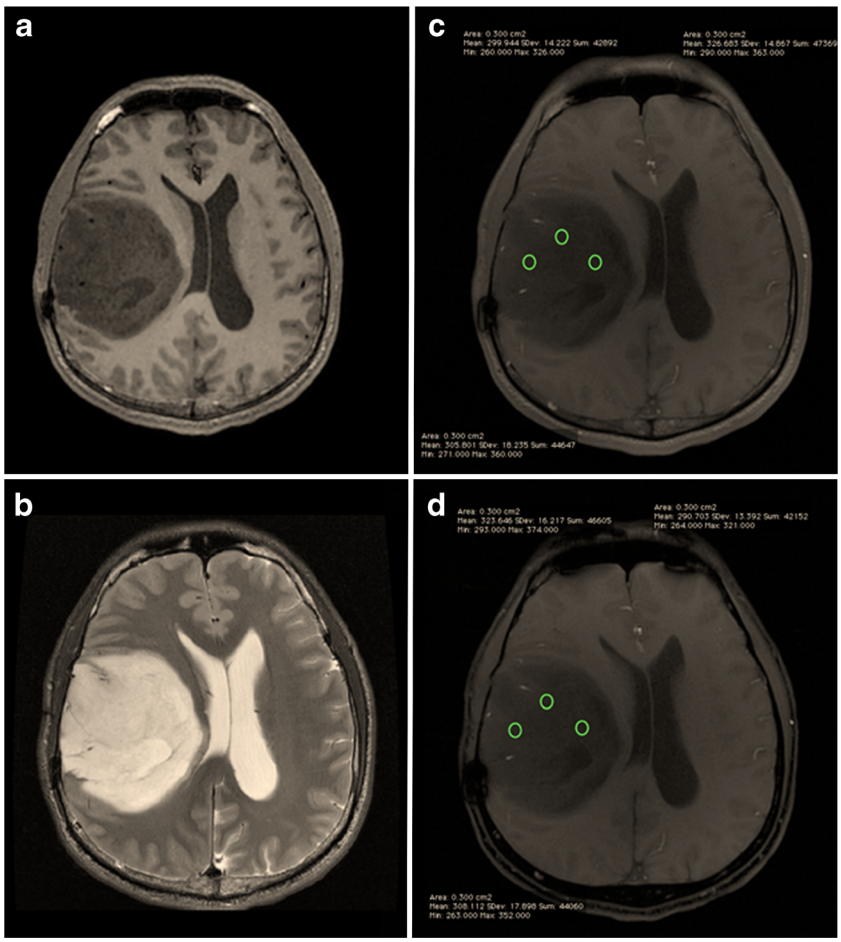

Fig. 2 Post-contrast T1W (a), T2W (b), in-phase (c) and opposed-phase (d) images of a grade II diffuse astrocytoma, with ROIs placed at the solid component

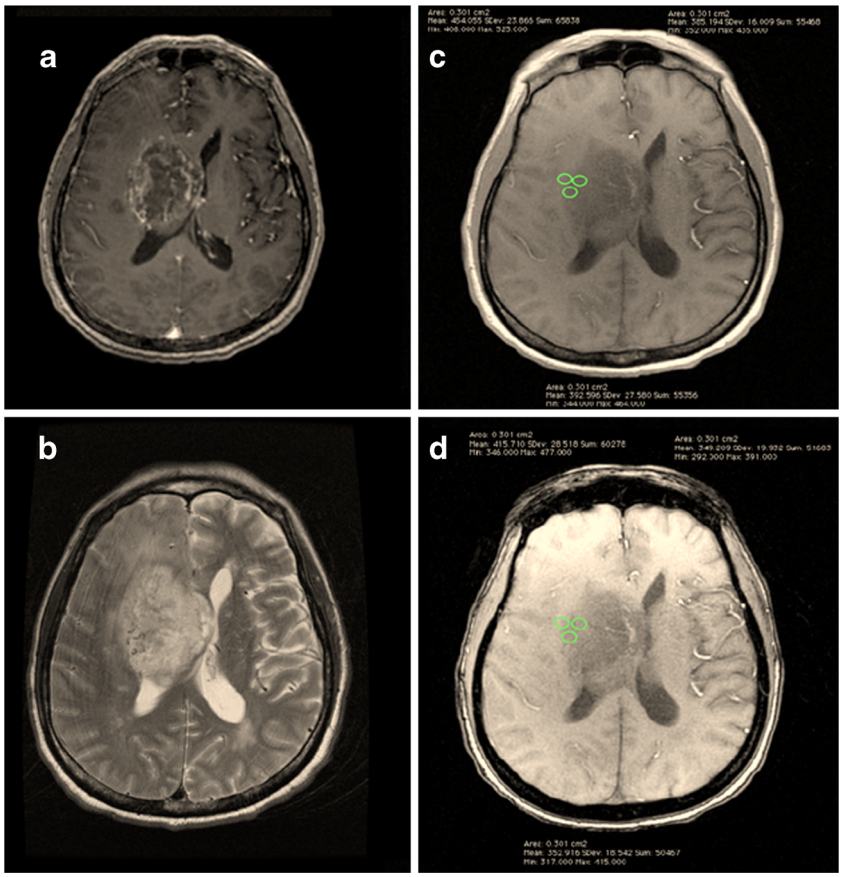

Fig. 3 Post-contrast T1W (a), T2W (b), in-phase (c) and opposed-phase (d) images of a grade IV GBM, with ROIs placed at the solid component

1.3 ppm (Lip1.3 ppm). A Pearson correlation test was run to determine the relationships between the lipid concentrations (in percentages), lipid components and SLR (Fig. 4). A positive correlation was found between lipid concentration and SLR (r=0.981, n=9, p<.001). Thus, large values of lipid concentrations are associated with large SLR values. There were statistically significant positive correlations between lipid concentration and Lip1.3 ppm (r=0.989, n=9, p<.001) and between lipid concentration and Lip0.9 ppm (r=0.789, n=9, p=0.011). Therefore, high lipid concentrations are associated

Table 1 Lipid concentrations from the phantom

Phantom	1 %		2 %		6 %		8 %		12 %		14 %		16 %		18 %		20 %		r
Lipid Components	Conc	SD %	Conc	SD %	Conc	SD %	Conc	SD %	Conc	SD %	Conc	SD %	Conc	SD %	Conc	SD %	Conc	SD %	
Lip0.9 ppm	0.002	3	0.002	3	0.009	3	0.009	3	0.015	4	0.017	3	0.020	4	0.013	8	0.049	4	0.789*
Lip1.3 ppm	0.009	1	0.014	1	0.044	1	0.053	1	0.088	1	0.111	1	0.134	1	0.169	1	0.162	2	0.989*
Lip2.02 ppm	0.001	6	0.001	6	0.003	5	0.004	6	0.005	6	0.006	5	0.009	7	0.002	20	-	>20	0.615
Lip2.23 ppm	0.001	6	0.001	5	0.004	4	0.004	5	0.005	5	0.007	5	0.011	6	0.004	14	-	>20	0.764*
Lip2.75 ppm	0.001	6	0.012	4	0.005	4	0.005	4	0.008	4	0.007	4	0.011	5	0.007	6	0.007	9	0.327
IOP																			
SLR	0.084		0.109		0.270		0.330		0.429		0.463		0.503		0.527		0.539		0.981*

Conc concentrations of lipid components resonating at that particular ppm, *SD* standard deviation, IOP opposed-phase imaging, *SLR* signal loss ratio obtained from IOP imaging, *r* Pearson correlation coefficient, correlating SLR and measured magnetic resonance spectroscopy (MRS) lipid component concentration

Measurements for bottles containing water were excluded from compliance with CRLB (Cramér–Rao lower bound), as all standard deviations were greater than 20 %

*Asterisks denote statistically significant difference (p<0.05) values for Pearson correlation test between lipid concentrations and lipid components

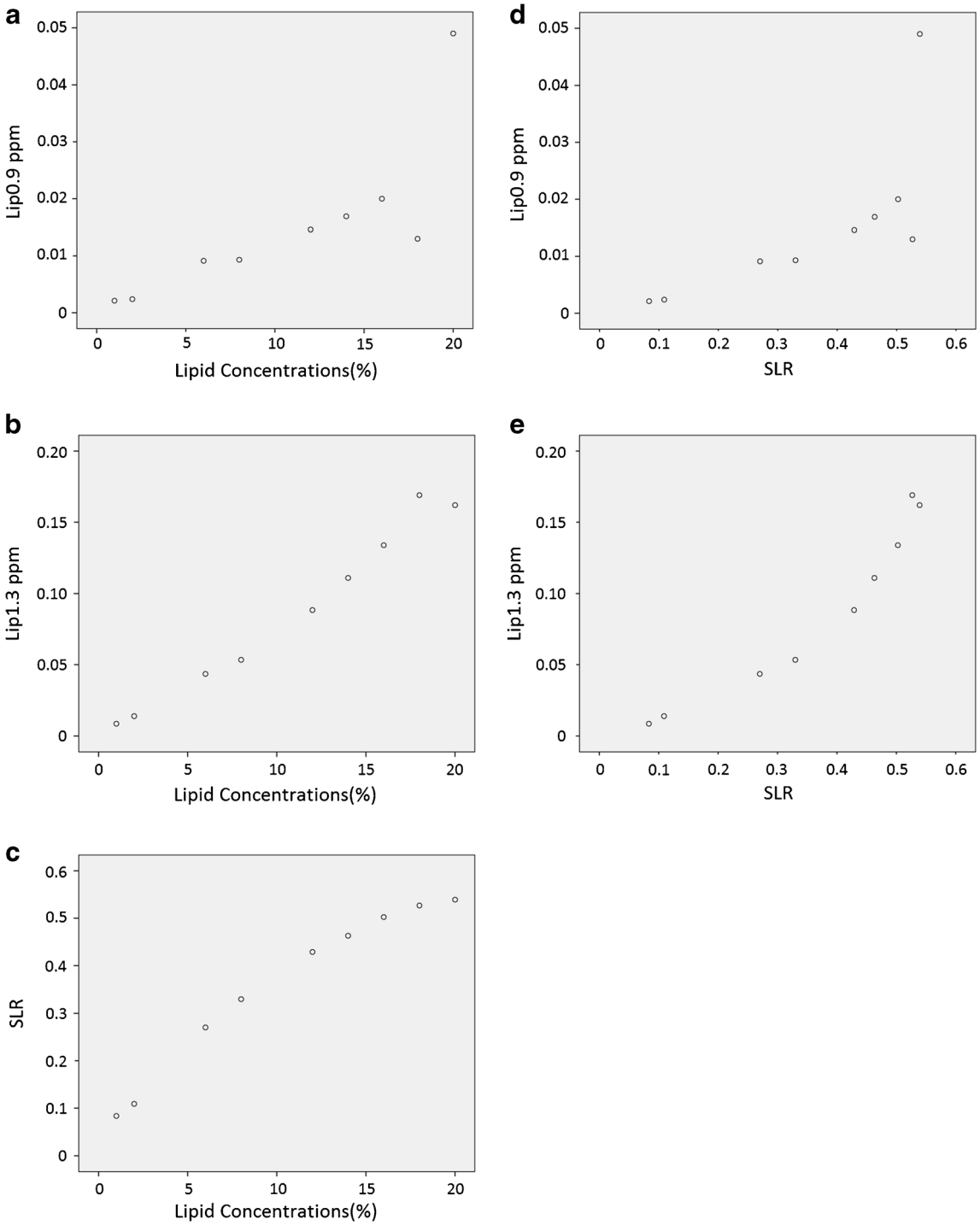

Fig. 4 Scatter plots showing relationships between lipid concentration (%) and (a) Lip0.9 ppm, (b) Lip1.3 ppm and (c) SLR. Scatter plots showing the relationship between SLR and (d) Lip0.9 ppm and (e) Lip1.3 ppm

with high concentrations of Lip0.9 ppm and Lip1.3 ppm. Similarly, strong positive correlations were depicted between SLR and Lip1.3 ppm (r=0.956, n=9, p<.001) and between SLR and Lip0.9 ppm (r=0.716, n=9, p=0.030), where high SLR is associated with high concentrations of Lip0.9 ppm and Lip1.3 ppm.

Clinical study

Demographic characteristics of the study population

The 22 patients with histologically proven glioma ranged in age from 10 to 71 years (14 male, 8 female). Nine patients

were diagnosed with grade II glioma, four with grade III glioma and nine with grade IV GBM. The median length of time between the MRI and histopathological examination was 0.84 months, and ranged from 1 day to 8 years. The median time delay was longer for grade II gliomas, as these patients were recruited on follow-up surveillance. Table 2 presents the demographic characteristics of the respondents.

Astrocytic tumours and tumour grading

Histological diagnoses included diffuse astrocytoma (n=5), pilomyxoid astrocytoma (n=1), gemistocytic astrocytoma (n=1), oligodendroglioma (n=1), anaplastic oligodendroglioma (n=4), oligoastrocytoma (n=1) and GBM (n=9). Two of the tumours were infratentorial in location (pilomyxoid astrocytoma in the right cerebellar vermis and diffuse astrocytoma in the brainstem) and the rest were located supratentorially. Grade II and III oligodendrogliomas were located in the frontal lobe (n=2), parietal lobe (n=3) and left basal ganglia (n=1). In contrast, the astrocytomas, including GBM, were found at various sites (involving all cerebral lobes but the occipital lobe), with five of the tumours demonstrating corpus callosum involvement (three were GBMs).

Descriptive analysis of MRS-detected lipids

Table 3 shows the descriptive data of various lipid components measured by LCModel, factored by WHO tumour grades II, III and IV. Lipids and macromolecules with peaks at Lip1.3a ppm, Lip2.0 ppm (lipid signals around 1.3 ppm and 2.0 ppm, respectively, in brain spectra) and Lip1.3a + Lip1.3b ppm (sum concentration of lipid signals resonating at 1.28–1.30 ppm) demonstrated statistically significant differences ($p<0.05$) across tumour grades (Table 3). The concentrations of Lip1.3a ppm and Lip1.3a + Lip1.3b ppm generally increased according to tumour grade. However, Lip2.0 ppm showed a slight dip from grade II to III, before increasing again from grade III to IV.

Analysis of the signal loss ratio in chemical shift IOP sequence

Table 4 shows the statistical descriptions and test results of SLR in the solid and cystic components of the tumours, factored by WHO tumour grades II, III and IV. Descriptive data are provided as median and inter-quartile range (IQR) values. Note that IQR values are not available for grade III, as there were only four patients with this grade. For the solid component, there was a general increase in SLR with increasing tumour grade, and a similar pattern was observed in the cystic component.

Comparison of classification probabilities between the two imaging techniques (SVS versus IOP imaging) in discriminating brain gliomas of different grades

The classification probabilities of the SVS and SLR were evaluated using three-group VUS analysis. VUS analysis is able to provide better accuracy for discriminating the three glioma grades (II, III and IV) than conventional binary class ROC analysis. Using the VUS method, we obtained VUS estimates and upper and lower cut-point values for the parameters measured (in this case, SVS and SLR). Higher VUS estimates indicate that the parameter has a higher discriminative power. Parameters with values smaller than the lower cut-points are classified as grade II, while those larger than the upper cut-points are classified as grade IV. Values within the upper and lower cut-points are classified as grade III. This method of analysis also provides the probability of correctly classifying the glioma grades.

Table 5 shows the VUS analysis on SVS and SLR. For SVS, only lipids and macromolecules with significant differences across tumour grades and with consistent increasing order across tumour grades were included in the analysis.

The distributions of lipid concentrations of Lip1.3a ppm and Lip1.3a + Lip1.3b ppm detected by LCModel according to the WHO actual grade are shown as boxplots in Fig. 5a and

Table 2 Patient demographics, with astrocytic tumours and tumour grading

Number of patients		Grade II 9	Grade III 4	Grade IV 9
Gender	Male	5 (55.6 %)	3 (75.0 %)	6(66.7 %)
	Female	4 (44.4 %)	1 (25.0 %)	3(33.3 %)
Age [mean (range), years]	Male	37.4 (15–61)	46.3 (24–67)	57.5 (42–71)
	Female	32.5 (17–45)	35.0 (35)	43.0 (10–65)
Tissue sampling (biopsy)	Total or partial resection	5	4	6
	Stereotactic biopsy	4	0	3
Time delay between MRS and histology [median (range), months]		2 (0.03–96.00)	1.5 (0.33–5.00)	0.6 (0.07–17.0)

Table 3 Median and IQR of lipid concentrations using SVS for WHO grade II to grade IV gliomas

Lipid Components	Grade II (n=9)		Grade III (n=3)		Grade IV (n=9)		Kruskal–Wallis
	Median	IQR	Median	IQR	Median	IQR	
Lip1.3a ppm	3.374	6.404	5.363	-	11.516	8.402	0.029*
Lip1.3b ppm	0.000	1.896	0.000	-	0.734	2.681	0.520
Lip0.9 ppm	2.033	1.737	1.112	-	3.681	3.36	0.050
MM0.9 ppm	1.402	2.561	3.226	-	1.732	1.939	0.232
Lip2.0 ppm	0.775	1.083	0.652	-	2.099	2.193	0.019*
MM2.0 ppm	2.135	2.839	3.028	-	2.160	4.652	0.890
MM1.2 ppm	0.525	0.655	0.642	-	0.483	0.834	0.827
MM1.4 ppm	0.584	2.499	2.226	-	0.300	2.792	0.584
MM1.7 ppm	0.507	0.883	2.020	-	0.684	1.169	0.278
Lip1.3a + Lip1.3b ppm	4.679	7.422	5.363	-	12.186	11.137	0.027*
MM1.4 + Lip1.3a + Lip1.3b + MM1.2 ppm	8.969	10.046	17.615	-	15.459	11.246	0.058
MM0.9 + Lip0.9 ppm	3.378	3.474	4.338	-	5.965	3.066	0.088
MM2.0 + Lip2.0 ppm	3.740	3.205	4.269	-	5.967	4.001	0.315

Descriptive data are provided as median and inter-quartile range (IQR) values. Note that there are no IQR values available for grade III, as there were only four patients with this grade

*p<0.05 across all tumour grades (grades II, III and IV), with the rightmost column showing the values of the Kruskal–Wallis tests

MRS results are not available for one grade III patient, owing to the poor quality of the spectra

b. The concentrations of Lip1.3a ppm and Lip1.3a + Lip1.3b ppm generally increase according to the tumour grade. Figure 5c and d depicts the distributions of signal loss ratios acquired from IOP imaging according to the WHO actual grade in the form of boxplots. The ratios of solid and cystic portions generally increase according to the tumour grade.

Discussion

Multiple studies have been conducted in efforts to develop a non-invasive method for the grading of gliomas. Most of these studies involved the utilization of both conventional and advanced MRI sequences, namely MRS, diffusion-weighted imaging (DWI), perfusion imaging and diffusion kurtosis imaging, in defining tumour morphology and glioma grade [2, 23].

Acknowledging the major role of lipids in tumour grading shown in previous studies [10, 13, 14], we addressed this issue by utilizing IOP sequences, which have a shorter acquisition time, in order to quantify the signal loss in proportion to the presence of lipid components. While previous phantom studies have used a fat–water interface method to obtain the fat fraction against the SI curve [8, 24, 25], our phantom uses water-soluble lipids to achieve lipid quantification. The presence of Lip0.9 ppm and Lip1.3 ppm depicted by MRS are reflected on the IOP images by means of SLR, as SVS was conducted on the phantom after the sequences were performed. This demonstrates that small lipid fractions are detectable by IOP imaging, thus representing a viable means of glioma detection in the clinical setting, as Lip0.9 ppm and Lip1.3 ppm have been reported to be associated with the diagnosis of glioma [3–6].

The lipid components obtained from SVS in the phantom study differed from those in the clinical study, as different basis sets were used. The phantom study used the special lipid settings to adjust for lipid and water components only, while the clinical study utilized standard brain spectra. The differences were obvious in terms of Lip1.3 ppm of the phantom

Table 4 SLR of solid and cystic components in grade II to grade IV glioma

	Grade II (n=9)		Grade III (n=4)		Grade IV (n=9)		Kruskal–Wallis
	Median	IQR	Median	IQR	Median	IQR	
Solid	0.040	0.034	0.089	-	0.098	0.037	0.001*
Cystic	0.018	0.048	0.081	-	0.093	0.063	0.033*

Note: rightmost columns showing the significant values of the Kruskal Wallis tests

Asterisks (*) denote statistically significant difference (p<0.05) values. *SLR* signal loss ratio

Table 5 Results of VUS analysis (non-parametric approach) for differentiating grades II, III and IV

Measurement	VUS	95 % CI	Lower cut-point	Upper cut-point	Correct classification probability		
					S_{II}	S_{III}	S_{IV}
Lip1.3a ppm	0.276	0.033–0.527	3.374	7.291	0.556	0.333	0.889
Lip1.3a + Lip1.3b ppm	0.350	0.092–0.667	4.679	7.685	0.556	0.333	0.889
SLR (solid)	0.639	0.291–0.904	0.064	0.086	1.000	0.500	0.889
SLR (cystic)	0.560	0.145–0.831	0.027	0.062	0.833	0.500	1.000

VUS volume under surface of the receiver operating characteristic curve (ROC), *CI* confidence interval, *SLR* signal loss ratio, S_{II} correct classification probability of grade II, S_{III} correct classification probability of grade III, S_{IV} correct classification probability of grade IV

MRS and Lip1.3a + Lip1.3b ppm obtained from clinical MRS. Lip1.3 ppm in the phantom study refers to a lipid signal around 1.3 ppm, whereas Lip1.3a + Lip1.3b ppm acquired from brain spectra resonates at 1.28–1.30 ppm, which was found to be enriched in neural stem cells [26].

Our clinical findings suggest that SLR can serve as a parameter for discriminating between glioma grades (II, III and IV). The SLR at the solid tumour portion was the best measure for differentiation, using optimal cut-points of 0.064 and 0.086, meaning that SLR values smaller than 0.064 are classified as grade II while SLR values larger than 0.086 are classified as grade IV. The values that lie between the cut-points are classified as grade III. Correct classification probability for grades II and IV was fairly high (S_{II} =1, S_{IV}=0.89), but was poorer for grade III (S_{III}=0.50), which may be due to the small sample size (n =4). A different approach was implemented for the evaluation of glioma grading, in which a three-group ROC analysis [21] was used rather than a typical binary ROC method, thus providing a more detailed analysis. To the best of our knowledge, there are no data yet available involving glioma studies using a three-group analysis approach.

This current study is the first to use this sequence for grading of intracranial glioma. Although some studies have evaluated the chemical shift sequence along with MRS [8, 27], the lipid types causing the signal loss were never proven to be similar to the lipid components identified in clinical MRS, due to MRS limitations related to intra-abdominal pathology. The limitation in the present study is the very small sample size, especially the grade III subsample. Because of the fast progression that occurs from grade III to grade IV, it was difficult to acquire grade III patients.

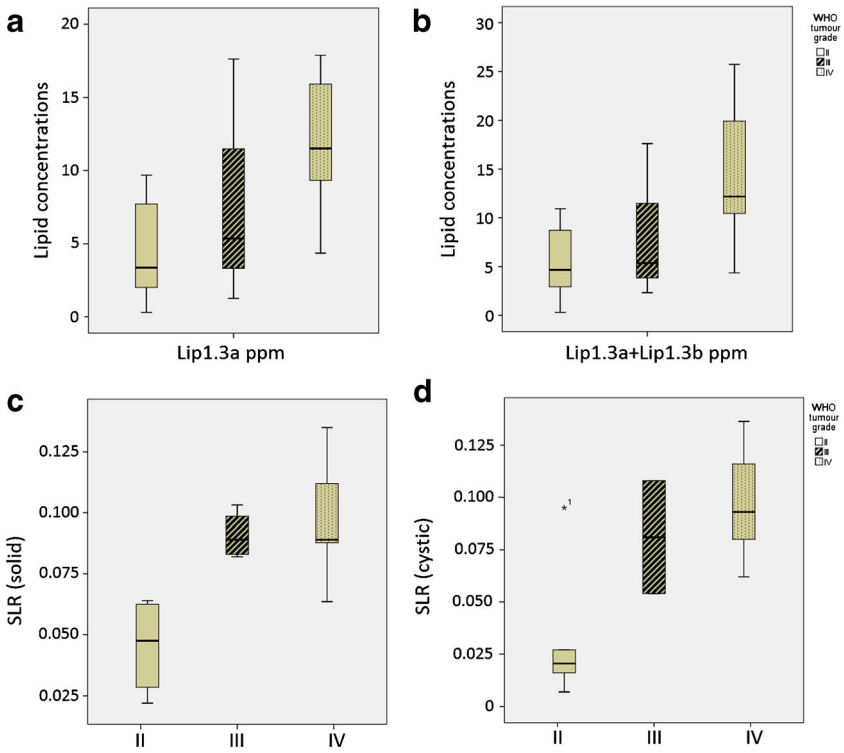

Fig. 5 Boxplots of lipid components acquired from MRS in different concentrations. (a) Lip1.3a ppm, (b) Lip1.3a + Lip1.3b ppm and SLR obtained from IOP imaging: (c) solid portion and (d) cystic portion of the tumour across WHO grade II to IV glioma

As this research study involves a novel MRI technique that was performed at a single institution, only a small population was studied. We propose a larger patient sample using multicentre participation to ensure a representative distribution of the population among which results will be generalized or transferred. Comparisons of the IOP method to other established methods such as diffusion-weighted imaging (DWI), perfusion imaging and diffusion kurtosis imaging in the grading and prognostication of glioma would also be advantageous.

Conclusions

The findings in this study provide a more comprehensive characterization of lipid quantification through the use of chemical shift GE IOP imaging, which may represent an alternative to the MRS technique. The chemical shift GE IOP imaging method supports the findings of previous studies revealing mobile lipids in higher-grade gliomas [14]. The three-group VUS analysis enabled a better evaluation of the discriminative ability of the SVS and SLR parameters among tumour grades (II, III and IV) compared to that of binary analysis (high grade vs. low grade) commonly performed in other studies [4–6]. This novel technique of using chemical shift GE IOP imaging has a promising future, with potential application for glioma staging in a research capacity.

Implications for patient care

This IOP sequence has the ability to grade gliomas with shorter imaging time than MRS. The IOP sequence may prove useful for patients who are unable to remain immobile in the scanner for long periods.

Acknowledgements This study was made possible with financial assistance from the University Malaya High Impact Research (HIR) Grant (J-20518-73808). The authors gratefully acknowledge the essential contributions of the research staff of University Malaya Research Imaging Centre (UMRIC). The study was presented as an oral presentation under novel techniques at the 2014 European Congress of Radiology in Vienna, Austria. The scientific guarantor of this publication is Prof. Dr. Norlisah Ramli. The authors of this manuscript declare no relationships with any companies whose products or services may be related to the subject matter of the article.

One of the authors has significant statistical expertise. Preparation of this manuscript were conducted with consultation of an expert in statistics, Mr. Tan Li Kuo, who is one of the authors of the manuscript. Institutional review board approval was obtained. Written informed consent was obtained from all subjects (patients) in this study. Methodology: cross sectional study, performed at one institution.

References

1. Hess KR, Broglio KR, Bondy ML (2004) Adult glioma incidence trends in the United States, 1977-2000. Cancer 101:2293–2299
2. Guzmán-De-Villoria JA, Mateos-Pérez JM, Fernández-García P, Castro E, Desco M (2014) Added value of advanced over conventional magnetic resonance imaging in grading gliomas and other primary brain tumors. Cancer Imaging 14:35
3. Bulik M, Jancalek R, Vanicek J, Skoch A, Mechl M (2013) Potential of MR spectroscopy for assessment of glioma grading. Clin Neurol Neurosurg 115:146–153
4. Kim JH, Chang KH, Na DG, Song IC, Kwon BJ, Han MH et al (2006) 3T 1H-MR spectroscopy in grading of cerebral glioma: comparison of short and intermediate echo time sequences. Am J Neuroradiol 27:1412–1418
5. Kousi E, Tsougos I, Tsolaki E, Fountas KN, Theodorou K, Fezoulidis I, Kapsalaki E, Kappas C (2012) Spectroscopic evaluation of glioma grading at 3T: the combined role of short and long TE. Sci World J 11
6. Law M, Yang S, Wang H, Babb JS, Johnson G, Cha S et al (2003) Glioma grading: sensitivity, specificity, and predictive values of perfusion MR imaging and proton MR spectroscopic imaging compared with conventional MR imaging. Am J Neuroradiol 24:1989–1998
7. Van Werven JR, Hoogduin JM, Nederveen AJ, Van Vliet AA, Wajs E, Vandenberk P et al (2009) Reproducibility of 3.0 Tesla magnetic resonance spectroscopy for measuring hepatic fat content. J Magn Reson Imaging 30:444–448
8. Namimoto T, Yasuyuki Y, Katsuhiko M, Yoshiharu N, Osamu M, Masataka K et al (2001) Adrenal masses: quantification of fat content with double-echo chemical shift in-phase and opposed-phase FLASH MR images for differentiation of adrenal adenomas. Radiology 218:642–646
9. Israel GM, Hindman N, Hecht E, Krinsky G (2005) The use of opposed-phase chemical shift MRI in the diagnosis of renal angiomyolipomas. AJR Am J Roentgenol 184:1868–1872
10. Outwater EK, Bhatia M, Siegelman ES, Burke MA, Mitchell DG (1997) Lipid in renal clear cell carcinoma: detection on opposed-phase gradient-echo MR Images. Radiology 205:103–107
11. Martin J, Sentis M, Zidan A, Donoso L, Puig J, Falco J et al (1995) Fatty metamorphosis of hepatocellular carcinoma: detection with chemical shift gradient-echo MR imaging. Radiology 195:125–130
12. Seiderer M, Staebler A, Wagner H (1999) MRI of bone marrow: opposed-phase gradient-echo sequences with long repetition time. Eur Radiol 9:652–661
13. Lim CJ, Ng KH, Ramli N, Azman RR (2011) Evaluation of the application of chemical shift for the detection of lipid in brain lesion. Radiography 17:43–48
14. Guo D, Bell EH, Chakravarti A (2013) Lipid metabolism emerges as a promising target for malignant glioma therapy. CNS Oncol 2: 289–299
15. Haase A, Frahm J, Matthaei D, Hanicke W, Merboldt KD (1986) FLASH imaging: rapid NMR imaging using low flip-angle pulses. J Magn Reson 67:258–266
16. Ragab Y, Ernad Y, Gheita T, Mansour M, Abou-Zeid A, Ferrari S et al (2009) Differentiation of osteoporotic and neoplastic vertebral fractures by chemical shift in-phase and out-of phase MR imaging. Eur J Radiol 72:125–133
17. Schindera ST, Soher BJ, Delong DM, Dale BM, Merkle EM (2008) Effect of echo time pair selection on quantitative analysis for

adrenal tumor characterization with in-phase and opposed-phase MR imaging: initial experience. Radiology 248:140–147
18. Gourtsoyiannis NC (2011) Clinical MRI of the abdomen: why, how, when, 1st edn. Springer-Verlag, Berlin
19. Provencher SW (2011) LCModel and LCMgui User's Manual
20. Cavassila S, Deval S, Huegen C, van Ormondt D, Graveron-Demilly D (2000) Cramer-Rao bound expressions for parametric estimation of overlapping peaks: influence of prior knowledge. J Magn Reson 143:311–320
21. Luo JQ, Xiong CJ (2012) DiagTest3Grp: an R package for analyzing diagnostic tests with three ordinal groups. J Stat Softw 51:3
22. Kleihues P, Louis DN, Scheithauer BW, Rorke LB, Reifenberger G, Burger PC et al (2002) The WHO classification of tumors of the nervous system. J Neuropathol Exp Neurol 61:215–225
23. Van Cauter S, De Keyzer F, Sima DM, Sava AC, D'Arco F, Veraart J et al (2014) Integrating diffusion kurtosis imaging, dynamic susceptibility-weighted contrast-enhanced MRI, and short echo time chemical shift imaging for grading gliomas. Neuro Oncol 16: 1010–1021
24. Merkle EM, Nelson RC (2006) Dual gradient-echo in-phase and opposed-phase hepatic MR imaging: a useful tool for evaluating more than fatty infiltration or fatty sparing. Radiographics 26:1409–1418
25. Opstad KS, Ladroue C, Bell BA, Griffiths JR, Howe FA (2007) Linear discriminant analysis of brain tumour (1)H MR spectra: a comparison of classification using whole spectra versus metabolite quantification. NMR Biomed 20:763–770
26. Park JH, Lee H, Makaryus R, Yu M, Smiths SD, Sayed K et al (2014) Metabolic profiling of dividing cells in live rodent brains by proton magnetic resonance spectroscopy (HMRS) and LCModel analysis. PLoS ONE 9:5
27. Chang JS, Taouli B, Salibi N, Hecht EM, Chin DG, Lee VS (2006) Opposed-phase MRI for fat quantification in fat-water phantoms with 1H MR spectroscopy to resolve ambiguity of fat or water dominance. AJR Am J Roentgenol 187:W103–W106